Deep EEG Source Localization via EMD-based fMRI High Spatial Frequency

Narges Moradi[a,b,c,*], Bradley G. Goodyear[b,c], Roberto C. Sotero[b,c]

[a]*Biomedical Engineering Graduate Program, University of Calgary, Calgary, AB, Canada,*
[b]*Department of Radiology, University of Calgary, Calgary, AB, Canada,*
[c]*Hotchkiss Brain Institute, University of Calgary, Calgary, AB, Canada,*

Abstract

Brain imaging with a high-spatiotemporal resolution is crucial for accurate brain-function mapping. Electroencephalography (EEG) and functional Magnetic Resonance Imaging (fMRI) are two popular neuroimaging modalities with complementary features that record brain function with high temporal and spatial resolution, respectively. One popular non-invasive way to obtain data with both high spatial and temporal resolutions is to combine the fMRI activation map and EEG data to improve the spatial resolution of the EEG source localization. However, using the whole fMRI map may cause spurious results for the EEG source localization, especially for deep brain regions. Considering the head's conductivity, deep regions' dipoles with low activity are unlikely to be detected by the EEG electrodes at the scalp. In this study, we use fMRI's high spatial-frequency component to identify the local high-intensity activations that are most likely to be captured by the EEG. The 3D Empirical Mode Decomposition (3D-EMD), a data-driven method, is used to decompose the fMRI map into its spatial-frequency components. Different validation measurements for EEG source localization show improved performance for the EEG inverse-modeling informed by the fMRI's high-frequency spatial component compared to the fMRI-informed EEG source-localization methods. The level of improvement varies depending on the voxels' intensity and their distribution.

Keywords: EMD-based EEG and fMRI integration, Deep EEG source localization, fMRI-informed EEG inverse modeling.

*Corresponding author: Narges Moradi (narges.moradi1@ucalgary.ca)
3330 Hospital Drive NW, HSC Building, Calgary, AB, T2N 4N1, Canada
Declarations of interest: none
Type of article: research paper

1. Introduction

Deep brain structures are critically important for brain function [1–4]. Thus, detecting the dipoles generated by the activity within deep regions is crucial for evaluating these regions' functions. Invasive techniques based on subdural electrodes are used to spot deep brain activity [1, 2, 5]. However, as these techniques are invasive, they could cause infection and other serious problems. Thus, a non-invasive yet accurate method is desired for localizing deep brain activity.

Electroencephalography (EEG) noninvasively records the electric potential produced by synchronous electrical dipoles in the brain. EEG sources are calculated by modeling the head layers with different conductivities and source currents using the quasi-static approximations of Maxwell's equations. However, finding the dipoles creating the scalp EEG signal is quite challenging and suffers from imprecision (typically in the order of centimeters) [6–9]. It is because, in addition to needing precise modeling of dipoles, head's conductivity, and noises, the number of possible dipoles outnumbers the EEG electrodes on the scalp. Consequently, there could be many dipole configurations that produce the same electric potential on the scalp [1, 9–12]. Moreover, localizing EEG signals arising from deep brain sources is usually more complex and is still under debate [1, 13].

Many EEG source-localization methods tend to assign sources of the recorded EEG signals to the dipoles on the cortical surface or have a low spatial resolution [1, 12, 14, 15]. Some methods, such as wMNE [16–18] and LORETA [19–21], have been proposed to reduce the effect of surface sources and improve the accuracy of specifying active dipoles in deep brain locations such as dipoles in the thalamus and hippocampus [20, 22]. wMNE method uses the column normalization of the lead-field matrix as a weighting matrix to compensate for the lower gains of deeper sources in the MNE method. On the other hand, LORETA assumes similarities between the current density of each cortex point to its neighbors and, thus maximum smoothness of the solution. In the LORETA method, a Laplacian operator is combined with the lead-field normalization of the wMNE method to ensure spatial coherence [1, 18, 20, 22]. However, each of these methods has its disadvantages. For instance, LORETA localizes deep sources smoother and better compared to the wMNE technique but provides lower spatial resolution, which is not good for the focal source estimation [1, 13, 15, 22, 23].

Scalp signals at the EEG electrodes are the combination of the captured signals from all the brain sources. Consequently, they contain various frequencies arising from different mechanisms underlying the neural activity [24]. It has been shown that focusing on EEG frequency bands separately and performing source localization for a single EEG band leads to more accurate results than the broadband EEG signal [25].

A popular way to specify deep activities is to guide EEG source localization by functional Magnetic Resonance Imaging (fMRI) data which is a noninvasive brain-imaging method with high spatial resolution. In this approach, EEG source localization results are affected by adding fMRI activation map information as a weight for locations that

are most likely to be active during a specific task and condition. Combining high-spatial-resolution data from fMRI with high-temporal-resolution data from EEG leads to data with a high spatial and temporal resolution [6, 7, 9, 26, 27]. The fMRI activation map can be used as a spatial constraint to solve the EEG-band inverse problem at a selected time window to investigate the brain-function dynamics [6–8].

A significant fMRI activation map is generated by the general linear model, considering conditions as regressors for the task-based data. For resting-state data, the fMRI-derived priors could be based on the changes in the correlation map in the resting-state networks [2, 28]. Voxels with changed functional connectivity in resting-state networks are considered active voxels in the fMRI map for resting-state data. Considering the fMRI map as a constraint should be done cautiously due to the mismatch between EEG and fMRI signals caused by the spatial extent of the BOLD signals around neuronal firing areas and signal detection failure [7, 8, 29, 30]. Consequently, EEG electrodes might not capture all the activity revealed on the fMRI map, especially in deep brain regions [2, 31–33]. Thus, considering the whole fMRI activation map as prior information on activated areas could cause spurious results for the EEG source localization.

As the EEG electrodes are placed on the scalp and due to the electrical conductivity of the head (transduction of the signals through the brain, cerebrospinal fluid, skull, and scalp), deep dipoles' electrical activity must be higher than a threshold to have a chance to be recorded by the EEG electrodes [2, 3, 5, 31–33]. Using fMRI's high spatial frequency components instead of the whole fMRI map provides more detailed spatial information on places with the local high activation [34]. High-intensity values on the fMRI map in deep brain regions are more likely to have enough signal-to-noise ratio (SNR) and be captured by the EEG electrodes [2, 31–33]. Moreover, in active areas, lower activation intensity and, accordingly, lower SNR around the highly activated voxels may reflect the spatial extent of the BOLD signals around neuronal firing spots [30]. Thus, fMRI high spatial frequency component- by specifying the local high-intensity voxels in active areas- spots the neuronal activities that are more likely to be recorded by the EEG electrodes.

In this study, we use the three-dimensional EMD method [35–37] to decompose each fMRI activation map into its Spatial Intrinsic Mode Functions (SIMFs). EMD is an adaptive and data-driven method that applies to any nonlinear and nonstationary data. Applying the 3D-EMD method [37] to the fMRI map extracts maps from high to low spatial frequencies. In the 3D-EMD method, the data's upper and lower envelopes are defined using the minima and maxima maps of the data. Subtracting the mean of the computed envelopes from the original data obtains the data's spatial components. These steps are repeated for the residual of the subtraction until there is no meaningful spatial frequency or variation to extract from the data (more details about this method can be found in [37]).

The first extracted SIMF that contains high spatial frequencies detects more abrupt changes, peaks, and valleys in the data and, therefore, more spatial details in the data.

In contrast, the higher SIMFs that contain lower frequencies show smoother variations. Therefore, high-frequency SIMF, by providing more details of the local spatial changes, helps to find dipoles of local maximum activation with more chance of their activation being captured by the EEG electrodes. We hypothesize that source-localizing EEG bands, constrained by the EMD-based [35, 36] fMRI's high-spatial-frequency map, provide more details with higher spatial accuracy about the activity of the sources. It primarily benefits the localization of deep dipoles, as they must have a relatively high intensity to pass different head layers and get to the electrodes on the head surface [5, 12]. Moreover, in patients with seizures, regions of higher-than-normal blood flow (fMRI intensity maximums) during a seizure may indicate where the seizure occurs [38]. Therefore, using the high SIMFs could assist in specifying a seizure starting point more accurately. Consequently, it improves the clinical interpretation of EEG signals and provides better diagnosis for different brain diseases.

Specifically, we add a weight coefficient computed from the map of the fMRI's high-frequency SIMFs to the EEG lead-field matrix. Weights with higher values show the locations with a higher probability of being the sources of the recorded EEG signals and vice versa [7]. The proposed method can be used as an accurate neuroimaging technique to unveil the brain sources' activity with high spatiotemporal resolution. We validate our approach using simulating EEG signals and the corresponding fMRI activation map. We evaluate how different activation intensities and distributions of an fMRI active area affect the source localization results of fMRI- and SIMF-informed EEG inverse modeling. We use measurements such as dipole localization error (DLE), Spatial Dispersion, and the F1-score to validate the proposed method and compare its results to the fMRI-informed EEG inverse modeling.

2. Method

2.1. Simulating EEG signals

We simulated EEG signals from two randomly selected sparse connected sources with frequencies of 5 Hz and sensor-level SNR of 4 dB for 90 subjects as follows:

$$\text{Signal}(t) = A(t)\sin(2\pi f t + \theta) + \text{Noise}, \tag{1}$$

where A and f are the amplitude and the frequency of the signal, t is the time, and θ is the starting phase of the signal. Narrow band noise is randomly added to each of the sources' signals. Then, the simulated source signal, which contains simulated sensor noise, is projected to the sensor space using the forward model. 128 scalp electrodes based on the 10−20 system and the volume-based BEM model [39] comprising of 13439 nodes (dipoles) were used to compute the lead field and the forward model. Thus, the source signal is multiplied by the lead field matrix for each source to forward project the source data to the sensor. The final sensor signal at each sensor is computed by summing up the resulting signals projected from all the source signals.

A standard MRI image with size $197 \times 233 \times 189$ was used to make the head model [40–42], and volume-based registration of the EEG sources to be accorded with the fMRI activation map. In this simulation, there was a correlation coefficient of 0.9 and 5 ms delays between the sources' time courses. We used SIMMEEG [42], a Matlab toolbox, to simulate the EEG signals.

2.2. Deriving priors from fMRI

We considered three active areas in the fMRI map. Two corresponded to the two EEG active sources, while the third one had no correspondence in the EEG activation map. fMRI values were randomly assigned within a corresponding spatial neighbourhood of each simulated EEG source to simulate fMRI active regions. We did not designate specific locations for the high-intensity voxels in the active areas. However, we put random values with a higher mean value for closer distances and with a lower mean value for farther distances. Figure 1 represents the locations of EEG sources, S1 and S2, which are also the center of the simulated fMRI active regions.

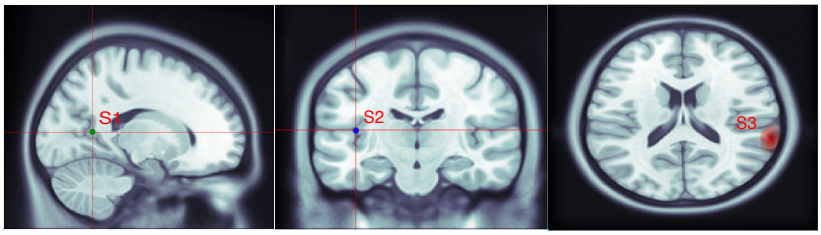

Figure 1: Locations of the simulated sources, S1, S2, and S3, are shown from left to right, respectively. Simulated EEG sources' subject-based coordinates are S1 = [82, 77, 82] and S2 = [57, 117, 84]. fMRI active regions are simulated in their spatial neighbourhood and comprise deep brain locations in the limbic lobe and posterior cingulate for S1, and sub-lobar, and insula, regions for S2. The fMRI extra source S3 is not related to any EEG source and comprises voxels in the temporal lobe and superior temporal areas.

The third active area in the fMRI activation map was simulated like the other two fMRI active regions, although it does not correspond to neuronal activity and is a representation of other processes in the brain, such as the maintenance of membrane potentials and neurotransmitter release and uptake. This is because there might be places detected as active in the fMRI map but not detectable in EEG recordings. These sources are referred to as "fMRI extra sources" [7, 8, 29]. S3 in Figure 1 demonstrates the location of the third activated area, the fMRI extra source, in the simulated fMRI map.

The fMRI-based constraints are added to the EEG inverse problem as a weight coefficient multiplied by the gain matrix. Thus, based on the fMRI activation map, a diagonal location-weighting matrix is computed with a size corresponding to the EEG head model and the lead field matrix used in the forward model. To compute fMRI's high spatial-frequency-based weights for EEG inverse modeling, we used the spatial EMD or 3D-EMD method to decompose the fMRI map into its spatial components [37].

Accordingly, the fMRI map is decomposed as follows:

$$\text{fMRI} = \sum_{i=1}^{n} \text{SIMF}_i + \text{Residue}, \tag{2}$$

where the first SIMF contains the highest changes of the fMRI activation map while the later SIMFs are smoother maps of spatial changes; the Residue represents the voxels' intensity trend in the fMRI map.

2.3. SIMF-informed EEG Inverse Modeling

EEG signals are projected back into the brain dipole current J via the inverse model as follows:

$$J = RG^T \left(GRG^T + \lambda C\right)^{-1} Y, \tag{3}$$

where G is the gain matrix, λ is the regularization parameter, C is the noise covariance matrix, and Y is the EEG recorded signals. The source-level covariance matrix R represents prior knowledge about the distribution of J [9]. R is usually assumed as an identity matrix, I, but applying fMRI data prior to EEG source localization, it is constructed according to weighting parameters computed from the fMRI map.

We used the first SIMF for making the diagonal SIMF-induced location-weighting matrix instead of the whole fMRI-induced weighting matrix to add to the EEG inverse problem. In the SIMF1, voxels with low fMRI intensities relative to their nearest high-intensity voxel in the fMRI map are considered not active to avoid weighting for the regions with weak fMRI signals that may not be caused by neuronal electrical activity and firing [30]. We then excluded voxels of intensity with less than half of the peak voxel intensity as their activity is unlikely to be captured by the EEG electrodes and, considering weak activities, add wrong weights to the EEG inverse model. It should be noted that, for real data, the threshold determining enough intensity for a voxel to be recorded on the scalp depends on the location of the voxel's region in the brain. For identifying low-activated voxels, the intensity of the voxel is added to its value in the residue (SIMF1+Residue) as the residue shows the intensity trend at voxels, and then the intensity threshold is applied.

We used the Brainstorm Matlab toolbox [43] to solve the EEG inverse problem and localize EEG sources constrained by the fMRI- and high-frequency SIMF-induced weights. In informed inverse modeling, large values for the weights derived from the fMRI and its SIMF activation map indicate more likely active locations. In contrast, small values indicate locations that are less likely to be active in EEG. Furthermore, to avoid spatially biased source localization by using the fMRI map as hard constraints, we put a weight of 0.1 instead of zero as a weight for the gain matrix of the EEG inverse model in not-activated areas in the fMRI map. The off-diagonal elements of R were set to zero [8].

In Brainstorm, we used the same volume head model to avoid errors and mislocalization caused by different head models during inverse and forward modeling. We examined how different activation intensities of the sources affect the source localization result. Figure 2 presents a schematic of applying the EMD-based-spatiotemporal fMRI constraints to the EEG source imaging.

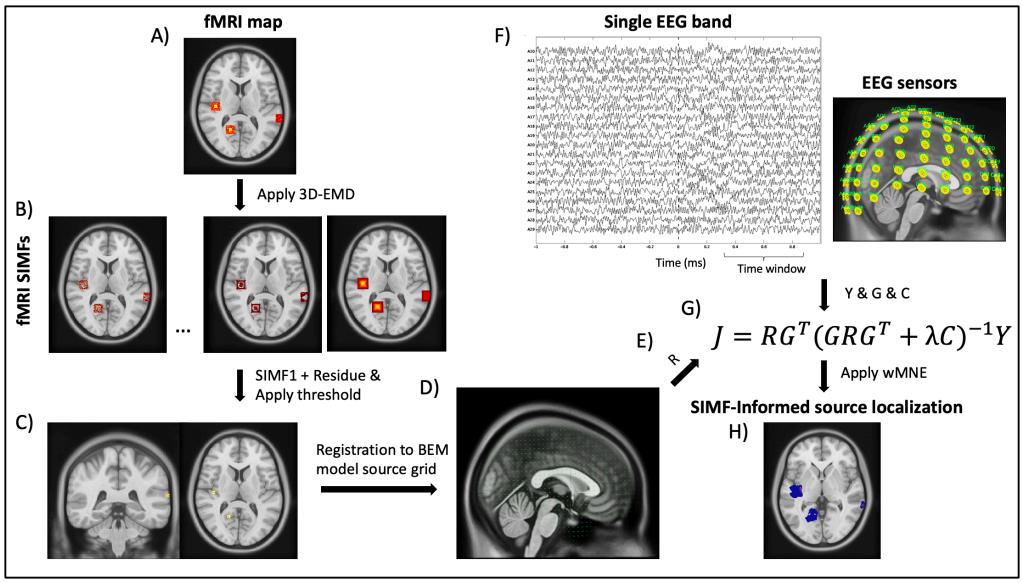

Figure 2: Schematic of SIMF-informed EEG source localization. High-frequency spatial components extracted from the fMRI map and the EEG signals recorded at the same condition are used for finding the activated sources with high spatial and temporal resolution. We start with computing the weighting matrix from the fMRI activation map. A) The 3D-EMD method is applied to the fMRI activation map to decompose it into its B) SIMFs. C) The local highly activated voxels are specified and after applying the activation threshold, D) they are registered to the same head model used for EEG inverse modeling. E) Each diagonal element of the weighting matrix R is computed according to its correspondence voxel activity in the fMRI activation map registered to the head model of the EEG inverse modeling. We used a weight of 0.1 for the dipoles in regions that are not activated based on the fMRI map. F) For a single EEG band (Y) recorded at EEG sensors, the gain matrix (G) and the covariance matrix (C) are computed. G) We solve the fMRI-informed-EEG inverse modeling equation by adding the diagonal weighting matrix R, computed from high-frequency SIMFs, as a coefficient for the gain matrix G. H) The SIMF-informed EEG source localization result is computed.

3. Results

The 3D-EMD method is applied to the fMRI map to decompose it into its SIMFs at each time window. Figure 3, demonstrates the application of the 3D-EMD on the fMRI map used in this study. For illustration purposes, we focused on one of the fMRI active zones to show the result of applying spatial EMD to the data and how the decomposed

SIMFs look like. SIMF1 is shown in Figure 3B and indicates that it can be used to locate the local high-intensity values in the fMRI map and to specify detailed intensity variation in the active area.

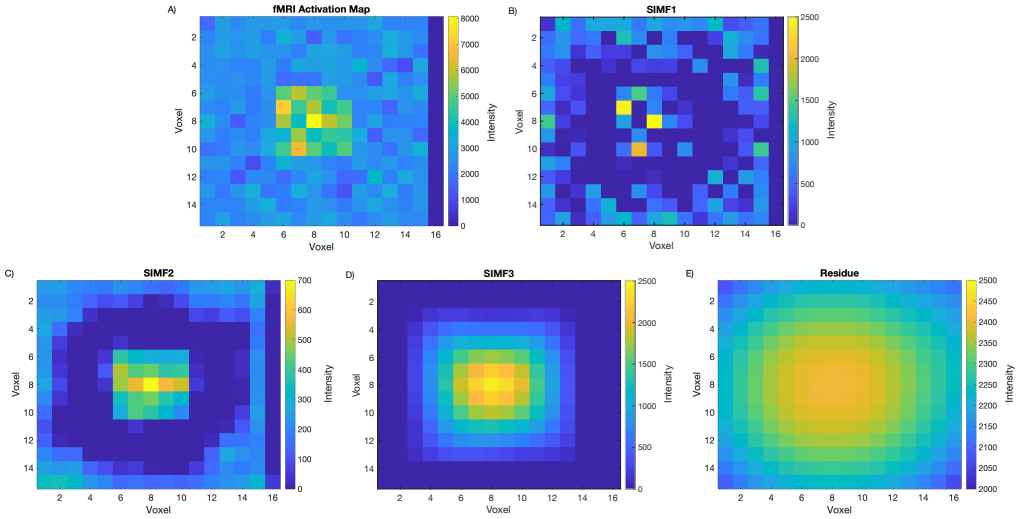

Figure 3: fMRI activation map and its SIMFs around one of the simulated sources. Figures demonstrate A) an fMRI active spot in the brain, B) SIMF1, C) SIMF2, D) SIMF3, and E) Residue, applying the 3D-EMD method. SIMF1 specifies the local maxima of fMRI intensities, and the residue presents the intensity trend of the fMRI activation map's voxels.

After source localization, we consider sources with a magnitude higher than 10 percent of the maximum intensity as a threshold [44]. To evaluate the proposed method and compare its results with the fMRI-informed EEG source localization, we compute DLE, Spatial Dispersion, and F1-score [13, 14, 45].

We compare the results of EEG source localization guided by the whole fMRI signal and the high spatial frequency of fMRI for simulated source configurations with different average intensities of the third active area. μ is the mean magnitude of the fMRI map at two of the active areas, and the mean magnitude of the third region is changed with respect to them. In this study, we consider different intensity distributions of the fMRI extra source as it makes more distinguishable changes in the validation measurement results compared to the cases where the true sources' intensities differ.

Table 1 shows the comparison of the DLE results for the fMRI- and SIMF-based EEG source localization for the same source configuration. It indicates that DLE values remain roughly the same with changing the mean intensity of the sources for fMRI-informed EEG-source localization. However, for SIMF-informed EEG source localization, the DLE values decrease by decreasing the mean intensity of sources. The lower DLE value represents the better performance of the SIMF-informed EEG source localization in specifying active sources more accurately and with lower localization errors.

Mean amplitude of fMRI extra active area	fMRI+EEG	SIMF1+EEG	Improvement (%)
1μ	33.5891 ± 0.2925	27.7011 ± 0.2765	17.5295%
0.8μ	34.0157 ± 0.3078	23.8480 ± 0.2726	29.8912%
0.3μ	35.5804 ± 0.3545	10.3789 ± 0.1335	70.8297%

Table 1: DLE for different fMRI extra active area's amplitude when the whole fMRI signal and high spatial frequencies of fMRI are considered as prior for EEG source localization with p-value < 0.05. Lower DLE means better source localization.

Table 2 presents the results of Spatial Dispersion for the same comparison as Table 1. For fMRI-informed EEG source localization, the Spatial Dispersion value decreases as the sources' mean intensity decreases. The lower values of the source intensities in the denominator of the Spatial Dispersion equation make it lower. However, for each source configuration, SIMF-informed EEG source localization shows significantly lower values for the Spatial Dispersion than the fMRI-informed EEG source localization, which represents the better performance of informing EEG source localization by the SIMF rather than the whole fMRI. Table 3 shows the F1-score results for the same comparisons and source configurations as Table 1 and Table 2. Although not much improvement is seen in terms of F1-score measurements, still, for each source configuration, F1-score for the SIMF-informed EEG source localization has a higher value than the fMRI-informed EEG source localization.

Mean amplitude of fMRI extra active area	fMRI+EEG	SIMF1+EEG	Improvement (%)
1μ	60.1786 ± 0.6162	58.1358 ± 0.6354	3.3945%
0.8μ	61.2021 ± 0.6160	54.8200 ± 0.6616	10.4279%
0.3μ	65.6162 ± 0.6005	32.9865 ± 1.1856	49.7281%

Table 2: Spatial Dispersion for different fMRI extra active area's amplitude when the whole fMRI signal and high spatial frequencies of fMRI are considered as prior for EEG source localization with p-value < 0.05. Lower Spatial Dispersion means better source localization.

Overall, results of the DLE, Spatial Dispersion, and F1-score show that informed source localization performs better and is more accurate when the high spatial frequencies of the fMRI activation map are used as prior information instead of the whole fMRI map. By lowering the mean of the fMRI activation intensity but keeping the same variance at the location of the third source with respect to the two other areas, results show lower DLE and Spatial Dispersion and higher F1-score applying the high-frequency SIMFs.

These results revealed the effect of the distribution of the voxels' intensities. An active area with high mean intensity has a smoother surface and variation compared to an active area with lower mean intensity and the same variance. Accordingly, for the first-mentioned active area, there might be a case that the active area does not even

have a SIMF to get extracted. However, the latter area with a lower mean has a relatively sparser and lower number of voxels with high enough SNR, which cause much difference between the activation map derived from high-frequency SIMF and the whole fMRI map. The sparser the distribution of high-intensity voxels, the more difference between the SIMF- and fMRI-based EEG source localization results.

Mean amplitude of fMRI extra active area	fMRI+EEG	SIMF1+EEG	Improvement (%)
1μ	0.8621 ± 0.0006	0.8816 ± 0.0005	2.2619%
0.8μ	0.8590 ± 0.0006	0.8956 ± 0.0005	4.2608%
0.3μ	0.8672 ± 0.0007	0.8891 ± 0.0007	2.5254%

Table 3: F1-score for different fMRI extra active area's amplitude when the whole fMRI signal and high spatial frequencies of fMRI are considered as prior for EEG source localization with p-value < 0.05. F1-score evaluates a method for identifying true activation. A higher value of the F1-score means better identification of the sources.

Figures 4 and 5, respectively, show an axial view of the results for fMRI-informed and high-frequency SIMF-informed EEG source localization when the mean intensity of the fMRI extra active area is 0.3 μ. Images from the top left to the bottom right indicate the result of each source localization from 0 to 996.1 ms with 66.5 ms apart.

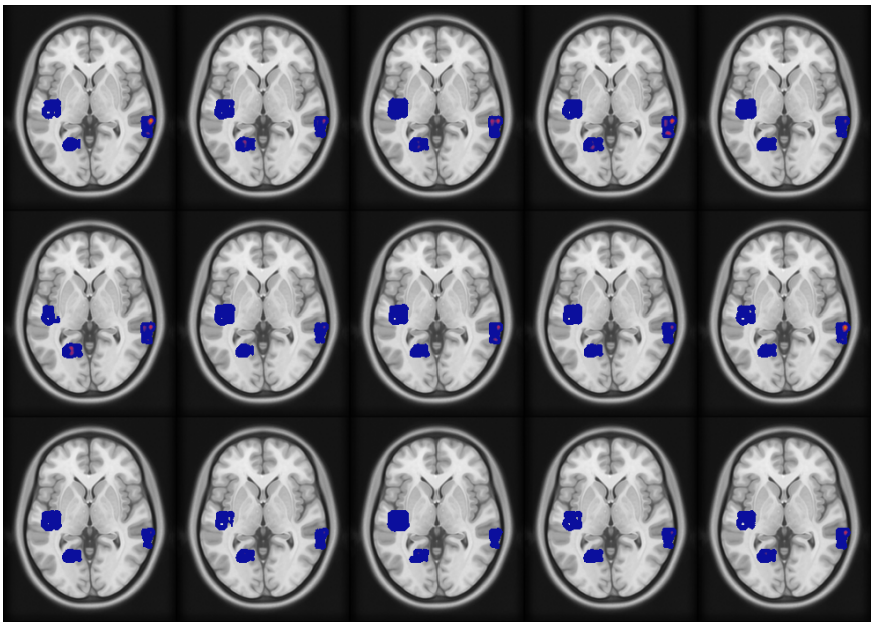

Figure 4: fMRI-informed source localization results when the mean intensity of the fMRI extra active area is 0.3 μ. Axial brain images from top left to bottom right show the sources' activity from 0 ms to 996.1 ms with 66.5 ms apart.

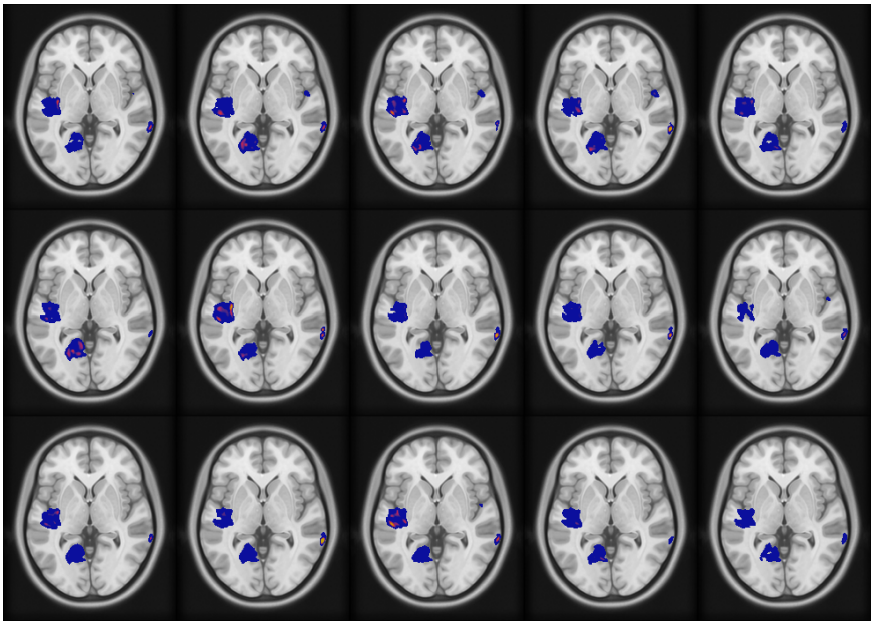

Figure 5: High-SIMF informed source localization results when the mean intensity of the fMRI extra active area is 0.3 μ. Axial brain images from top left to bottom right demonstrate the sources' activity from 0 ms to 996.1 ms with 66.5 ms apart.

Of note, as the two simulated EEG sources are in deep brain regions, uninformed EEG inverse modeling would show activity in the majority of surface brain areas. However, adding fMRI weight to the inverse model helps to find deep activated sources more accurately. Applying SIMF1-induced weights instead of whole fMRI data improves localizing sources' activity by locating sparser and more accurate highly active dipoles with more spatial details and, consequently, higher spatial resolution.

It should be mentioned that we can compute fMRI-based priors for a specific time window of interest in the EEG data, which makes them time-variant fMRI constraints. It has been shown that EEG inverse modeling informed by static fMRI constraints may cause inaccurate or erroneous results [27].

4. Discussion

In this paper, we show that using the high spatial components (SIMF) of an fMRI map as a spatial constraint for the EEG source localization improves the accuracy of specifying active dipoles. This approach is effective for localizing deep brain active dipoles, which their activities play a pivotal role in central nervous system functioning. Due to the different head-layers conductivities, electrical potential from deep dipoles can be captured by EEG electrodes on the scalp if their power is high enough. The larger the depth is, the weaker the source affects the scalp signal. Applying the data-driven

3D-EMD method, fMRI map data recorded at the same condition as EEG recording is decomposed into its spatial components (SIMFs). Information from high-frequency SIMF that spot voxels with the local high-activation is added to the EEG inverse model as a weight to avoid the bias of EEG inverse modeling toward surface dipoles.

Specifically, EEG source localization methods mostly fail to localize deep brain dipoles [1, 12–15]. They relate the recorded potential to the low-intensity dipoles on the brain surface instead of high-intensity dipoles in the deep regions like the insula and thalamus [1, 12–15]. EEG sources are congruent with the hemodynamic changes measured by fMRI. One widely used method to improve this performance impairment of the EEG inverse modeling is using the fMRI map data, which is of high spatial resolution as priors for constraining EEG source space [10, 46, 47]. Thus, several studies have used EEG and fMRI data recorded during the same task or simultaneously in a resting state to yield data with high spatial and temporal resolution [6–9, 26–28].

However, using the whole fMRI data may cause spurious results because all the activities of the activated regions on the fMRI map cannot be captured by EEG electrodes on the scalp. They might not have enough SNR (especially problematic for active deep brain regions) or not be generated by neuronal firing. The first issue is caused by the requirement that neural activity in deep regions, mapped in fMRI, must have an intensity higher than a threshold, depending on the different brain layers' conductivity, to be recorded by the scalp electrodes. The second issue might be caused by the spatial extent of the BOLD signals, which appear as voxels with low SNR around highly activated voxels.

Subcortical regions are mediators for the brain networks' communication as they are anatomically connected to an extensive part of cortical regions. Deep regions process primitive functions such as sleep, wakefulness, consciousness, learning, and memory [1–4]. It has been shown in Refs. [2, 48] subcortical structures, such as the amygdala and thalamus, and some parts of the hippocampus, such as the dentate gyrus, have relatively high source density compared to other regions in the neocortex. Thus, a small active volume in these regions is enough to produce a high-power signal to be detected by the scalp electrodes. Thereby, we use fMRI's high-frequency SIMFs instead of applying the whole fMRI map, to spot more sparse and localized regions with voxels of high-intensity power that are more probable to be captured by the EEG electrodes. Consequently, weighting the lead-filed matrix of the EEG inverse model based on these high-frequency SIMFs leads to more accurate results with higher resolution.

We compared the SIMF-based EEG inverse modeling performance with the fMRI-based EEG inverse modeling. Results demonstrated that using SIMF as a prior constraint makes the EEG inverse modeling more accurate and localizes sources sparser compared to other methods. More accurate source localization means the proposed method provides higher spatial resolution data of neural activity [49].

Furthermore, we considered the fMRI-extra source in our computations for the EEG inverse modeling. There is also a case where we might have an EEG-extra or fMRI-

invisible source. EEG-extra source is either active for a short time or is from a few neurons that cannot make significant and detectable metabolism changes to be appeared in fMRI [50]. It has been shown in Refs. [8, 51] that for including the EEG-extra source, we need to find the proper and high enough value as a coefficient for the fMRI-induced weight matrix that lets the EEG-extra source be visible in inverse modeling. Thus, the whole process will be the same as when there is no EEG-extra source, except that after applying the high-spatial-frequency-induced weight, we find a constant value to be multiplied by the whole lead-field matrix that is large enough to balance the weight coefficient matrix.

It is of note that the proposed method can be used for resting state data as well as task. It has been shown in Ref. [34] that resting-state functional connectivity computed based on the high-frequency fMRI's SIMFs is more precise than based on the whole fMRI data. Each resting-state brain network computed from resting-state fMRI data is associated with a specific combination of EEG bands [28]. Thus, we can localize the sources that cause variations in the resting-state EEG bands connectivity pattern by adding weights for grids corresponding to the highly activated voxels at regions in which the fMRI connectivity map has been changed.

Moreover, it has been demonstrated that the fMRI Blood Oxygenation Level Dependent (BOLD) signal is associated with neuronal synchronization across EEG frequency bands (i.e., neurovascular coupling). The powers of the alpha (8-12 Hz) and beta (12-30 Hz) bands correlate negatively with BOLD signal magnitude, while the gamma band (> 30 Hz) power correlates positively with BOLD signal magnitude [24, 52–54]. Thus, after computing the significant fMRI activation map, the association between the fMRI BOLD signal with neuronal synchronization across EEG frequency bands (i.e., neurovascular coupling) could be used as an extra filter for specifying fMRI-based weights added to the EEG inverse problem.

In summary, for most EEG inverse modeling methods, recovering deep sources is problematic and challenging as dipoles located at the brain surface with low-intensity power are privileged. The proposed approach adds information from the EMD-based fMRI's high spatial frequency components as a weight to the EEG inverse modeling to solve the bias against deep brain sources and accurately image dynamic neural activity with higher spatial resolution. Higher spatial and temporal resolution maps of neural activity improve our brain function knowledge. Precise brain activity localization helps us find more effective treatments for brain diseases such as ADHD and epilepsy by providing substantial information about the source of the epileptogenic process and distinguishing patterns of ADHD [1, 38, 55].

5. Acknowledgement

This work was supported by grant number RGPIN-2022-03042 from the Natural Sciences and Engineering Research Council of Canada.

References

[1] S. Asadzadeh, T. Yousefi Rezaii, S. Beheshti, A. Delpak, and S. Meshgini. A systematic review of EEG source localization techniques and their applications on diagnosis of brain abnormalities. *J. Neurosci. Methods*, 339:108740, 2020. doi:10.1016/j.jneumeth.2020.108740.

[2] M. Fahimi Hnazaee, B. Wittevrongel, E. Khachatryan, A. Libert, E. Carrette, I. Dauwe, A. Meurs, P. Boon, D. Van Roost, and M. M. Van Hulle. Localization of deep brain activity with scalp and subdural EEG. *Neuroimage*, 223:117344, 2020. doi:10.1016/j.neuroimage.2020.117344.

[3] M. Seeber, L. M. Cantonas, M. Hoevels, T. Sesia, V. Visser-Vandewalle, and C. M. Michel. Subcortical electrophysiological activity is detectable with high-density eeg source imaging. *Nat. Commun.*, 10(1):753, 2019. doi:10.1038/s41467-019-08725-w.

[4] M. W. Cole, S. Pathak, and W. Schneider. Identifying the brain's most globally connected regions. *Neuroimage*, 49(4):3132–48, 2010. doi:10.1016/j.neuroimage.2009.11.001.

[5] E. D. Farahani, J. Wouters, and A. van Wieringen. Contributions of non-primary cortical sources to auditory temporal processing. *Neuroimage*, 191:303–314, 2019. doi:10.1016/j.neuroimage.2019.02.037.

[6] M. J. Rosa, J. Daunizeau, and K. J. Friston. EEG-fMRI integration: a critical review of biophysical modeling and data analysis approaches. *J. Integr. Neurosci.*, 9(4):453–76, 2010. doi:10.1142/s0219635210002512.

[7] Jean Daunizeau, Christophe Grova, Jérémie Mattout, Guillaume Marrelec, Diego Clonda, Bernard Goulard, Mélanie Pélégrini-Issac, J-M Lina, and Habib Benali. Assessing the relevance of fmri-based prior in the EEG inverse problem: a bayesian model comparison approach. *IEEE Transactions on Signal Processing*, 53(9):3461–3472, 2005.

[8] A. K. Liu, J. W. Belliveau, and A. M. Dale. Spatiotemporal imaging of human brain activity using functional mri constrained magnetoencephalography data: Monte carlo simulations. *Proc Natl Acad Sci U S A*, 95(15):8945–50, 1998. doi:10.1073/pnas.95.15.8945.

[9] Hailing Wang, Xu Lei, Zhichao Zhan, Li Yao, and Xia Wu. A new fMRI informed mixed-norm constrained algorithm for EEG source localization. *IEEE Access*, 6:8258–8269, 2018.

[10] M. Zhu, W. Zhang, D. L. Dickens, and L. Ding. Reconstructing spatially extended brain sources via enforcing multiple transform sparseness. *Neuroimage*, 86:280–93, 2014. doi:10.1016/j.neuroimage.2013.09.070.

[11] Sylvain Baillet, John C Mosher, and Richard M Leahy. Electromagnetic brain mapping. *IEEE Signal processing magazine*, 18(6):14–30, 2001.

[12] Stanislas Lagarde and Fabrice Bartolomei. Focal epilepsies and focal disorders. *Handbook of Clinical Neurology*, 161:17–43, 2019.

[13] Chen Wei, Kexin Lou, Zhengyang Wang, Mingqi Zhao, Dante Mantini, and Quanying Liu. Edge sparse basis network: a deep learning framework for EEG source localization. In *2021 International Joint Conference on Neural Networks (IJCNN)*, pages 1–8. IEEE, 2021.

[14] O. Hauk, D. G. Wakeman, and R. Henson. Comparison of noise-normalized minimum norm estimates for MEG analysis using multiple resolution metrics. *Neuroimage*, 54(3):1966–74, 2011. doi:10.1016/j.neuroimage.2010.09.053.

[15] J. Yao and J. P. Dewald. Evaluation of different cortical source localization methods using simulated and experimental EEG data. *Neuroimage*, 25(2):369–82, 2005. doi:10.1016/j.neuroimage.2004.11.036.

[16] M. S. Hamalainen and R. J. Ilmoniemi. Interpreting magnetic fields of the brain: minimum norm estimates. *Med. Biol. Eng. Comput.*, 32(1):35–42, 1994. doi:10.1007/BF02512476.

[17] J. Z. Wang, S. J. Williamson, and L. Kaufman. Magnetic source images determined by a lead-field analysis: the unique minimum-norm least-squares estimation. *IEEE Trans. Biomed. Eng.*, 39(7):665–75, 1992. doi:10.1109/10.142641.

[18] Sunao Iwaki and Shoogo Ueno. Weighted minimum-norm source estimation of magnetoencephalog-

raphy utilizing the temporal information of the measured data. *Journal of Applied physics*, 83(11):6441–6443, 1998.

[19] J. F. Lubar, M. Congedo, and J. H. Askew. Low-resolution electromagnetic tomography (LORETA) of cerebral activity in chronic depressive disorder. *Int J Psychophysiol*, 49(3):175–85, 2003. doi:10.1016/s0167-8760(03)00115-6.

[20] R. D. Pascual-Marqui, C. M. Michel, and D. Lehmann. Low resolution electromagnetic tomography: a new method for localizing electrical activity in the brain. *Int. J. Psychophysiol*, 18(1):49–65, 1994. doi:10.1016/0167-8760(84)90014-x.

[21] R. D. Pascual-Marqui. Standardized low-resolution brain electromagnetic tomography (sLORETA): technical details. *Methods Find Exp Clin Pharmacol*, 24 Suppl D:5–12, 2002. URL: https://www.ncbi.nlm.nih.gov/pubmed/12575463.

[22] R. Grech, T. Cassar, J. Muscat, K. P. Camilleri, S. G. Fabri, M. Zervakis, P. Xanthopoulos, V. Sakkalis, and B. Vanrumste. Review on solving the inverse problem in EEG source analysis. *J Neuroeng Rehabil*, 5:25, 2008. doi:10.1186/1743-0003-5-25.

[23] Michael J. Aminoff and Robert B. Daroff. *Encyclopedia of the neurological sciences*. Academic Press/Elsevier, Waltham, MA, second edition. edition, 2014.

[24] R. Scheeringa, P. Fries, K. M. Petersson, R. Oostenveld, I. Grothe, D. G. Norris, P. Hagoort, and M. C. Bastiaansen. Neuronal dynamics underlying high- and low-frequency EEG oscillations contribute independently to the human bold signal. *Neuron*, 69(3):572–83, 2011. doi:10.1016/j.neuron.2010.11.044.

[25] K. Al-Subari, S. Al-Baddai, A. M. Tomé, G. Volberg, B. Ludwig, and E. W. Lang. Combined EMD-sLORETA analysis of EEG data collected during a contour integration task. *PLoS One*, 11(12):e0167957, 2016. doi:10.1371/journal.pone.0167957.

[26] Christoph Mulert and Louis Lemieux. *EEG-fMRI: physiological basis, technique, and applications*. Springer Science & Business Media, 2009.

[27] T. Nguyen, T. Potter, C. Karmonik, R. Grossman, and Y. Zhang. EEG source imaging guided by spatiotemporal specific fMRI: Toward an understanding of dynamic cognitive processes. *Neural Plast*, 2016:4182483, 2016. doi:10.1155/2016/4182483.

[28] D. Mantini, M. G. Perrucci, C. Del Gratta, G. L. Romani, and M. Corbetta. Electrophysiological signatures of resting state networks in the human brain. *Proceedings of the National Academy of Sciences*, 104(32):13170–13175, 2007. doi:10.1073/pnas.0700668104.

[29] R. N. Henson, D. G. Wakeman, V. Litvak, and K. J. Friston. A parametric empirical bayesian framework for the EEG/MEG inverse problem: Generative models for multi-subject and multi-modal integration. *Front Hum. Neurosci*, 5:76, 2011. doi:10.3389/fnhum.2011.00076.

[30] Z. S. Saad, K. M. Ropella, E. A. DeYoe, and P. A. Bandettini. The spatial extent of the BOLD response. *Neuroimage*, 19(1):132–44, 2003. doi:10.1016/s1053-8119(03)00016-8.

[31] D. Cosandier-Rimélé, F. Bartolomei, I. Merlet, P. Chauvel, and F. Wendling. Recording of fast activity at the onset of partial seizures: depth EEG vs scalp EEG. *Neuroimage*, 59(4):3474–87, 2012. doi:10.1016/j.neuroimage.2011.11.045.

[32] Wilder Penfield and Herbert Jasper. *Epilepsy and the functional anatomy of the human brain.* Little, Brown & Co., 1954.

[33] G. Ramantani, L. Maillard, and L. Koessler. Correlation of invasive EEG and scalp EEG. *Seizure*, 41:196–200, 2016. doi:10.1016/j.seizure.2016.05.018.

[34] N. Moradi, M. Dousty, and R. C. Sotero. Spatiotemporal empirical mode decomposition of resting-state fMRI signals: Application to global signal regression. *Front. Neurosci.*, 13:736, 2019. doi:10.3389/fnins.2019.00736.

[35] Norden E Huang and Samuel S P Shen. *Hilbert-Huang transform and its applications*, volume 16. World Scientific, 2005.

[36] Norden E Huang, Zheng Shen, Steven R Long, Manli C Wu, Hsing H Shih, Quanan Zheng, Nai-Chyuan Yen, Chi Chao Tung, and Henry H Liu. The empirical mode decomposition and the hilbert spectrum for nonlinear and non-stationary time series analysis. *Proceedings of the Royal Society of*

London. Series A: mathematical, physical and engineering sciences, 454(1971):903–995, 1998.

[37] Jamal Riffi, Adnane Mohamed Mahraz, Abdelghafour Abbad, and Hamid Tairi. 3d extension of the fast and adaptive bidimensional empirical mode decomposition. *Multidimensional Systems and Signal Processing*, 26(3):823–834, 2015.

[38] M. Zhao, J. Nguyen, H. Ma, N. Nishimura, C. B. Schaffer, and T. H. Schwartz. Preictal and ictal neurovascular and metabolic coupling surrounding a seizure focus. *J. Neurosci.*, 31(37):13292–300, 2011. doi:10.1523/JNEUROSCI.2597-11.2011.

[39] M. Fuchs, R. Drenckhahn, H. A. Wischmann, and M. Wagner. An improved boundary element method for realistic volume-conductor modeling. *IEEE Trans. Biomed. Eng.*, 45(8):980–97, 1998. doi:10.1109/10.704867.

[40] A. Gramfort, T. Papadopoulo, E. Olivi, and M. Clerc. OpenMEEG: opensource software for quasistatic bioelectromagnetics. *Biomed. Eng. Online*, 9:45, 2010. doi:10.1186/1475-925X-9-45.

[41] J. Kybic, M. Clerc, T. Abboud, O. Faugeras, R. Keriven, and T. Papadopoulo. A common formalism for the integral formulations of the forward EEG problem. *IEEE Trans. Med. Imaging*, 24(1):12–28, 2005. doi:10.1109/tmi.2004.837363.

[42] A. T. Herdman. SimMEEG software for simulating event-related MEG and EEG data with underlying functional connectivity. *J. Neurosci. Methods*, 350:109017, 2021. doi:10.1016/j.jneumeth.2020.109017.

[43] F. Tadel, S. Baillet, J. C. Mosher, D. Pantazis, and R. M. Leahy. Brainstorm: a user-friendly application for MEG/EEG analysis. *Comput. Intell. Neurosci.*, 2011:879716, 2011. doi:10.1155/2011/879716.

[44] J. H. Cho, S. B. Hong, Y. J. Jung, H. C. Kang, H. D. Kim, M. Suh, K. Y. Jung, and C. H. Im. Evaluation of algorithms for intracranial EEG (iEEG) source imaging of extended sources: feasibility of using iEEG source imaging for localizing epileptogenic zones in secondary generalized epilepsy. *Brain Topogr*, 24(2):91–104, 2011. doi:10.1007/s10548-011-0173-2.

[45] K. Whittingstall, G. Stroink, L. Gates, J. F. Connolly, and A. Finley. Effects of dipole position, orientation and noise on the accuracy of EEG source localization. *Biomed. Eng. Online*, 2:14, 2003. doi:10.1186/1475-925X-2-14.

[46] Jean-Philippe Lachaux, Pierre Fonlupt, Philippe Kahane, Lorella Minotti, Dominique Hoffmann, Olivier Bertrand, and Monica Baciu. Relationship between task-related gamma oscillations and BOLD signal: New insights from combined fMRI and intracranial EEG. *Human Brain Mapping*, 28(12):1368–1375, 2007. doi:10.1002/hbm.20352.

[47] X. Lei, P. Xu, C. Luo, J. Zhao, D. Zhou, and D. Yao. fMRI functional networks for EEG source imaging. *Hum. Brain Mapp.*, 32(7):1141–60, 2011. doi:10.1002/hbm.21098.

[48] D. Keller, C. Erö, and H. Markram. Cell densities in the mouse brain: A systematic review. *Front Neuroanat*, 12:83, 2018. doi:10.3389/fnana.2018.00083.

[49] Teresa Jacobson Kimberley and Scott M Lewis. Understanding neuroimaging. *Physical therapy*, 87(6):670–683, 2007.

[50] K. Friston, L. Harrison, J. Daunizeau, S. Kiebel, C. Phillips, N. Trujillo-Barreto, R. Henson, G. Flandin, and J. Mattout. Multiple sparse priors for the M/EEG inverse problem. *Neuroimage*, 39(3):1104–20, 2008. doi:10.1016/j.neuroimage.2007.09.048.

[51] S. Samadi, H. Soltanian-Zadeh, and C. Jutten. Integrated analysis of EEG and fMRI using sparsity of spatial maps. *Brain Topogr*, 29(5):661–78, 2016. doi:10.1007/s10548-016-0506-2.

[52] Y. Murayama, F. Biessmann, F. C. Meinecke, K. R. Müller, M. Augath, A. Oeltermann, and N. K. Logothetis. Relationship between neural and hemodynamic signals during spontaneous activity studied with temporal kernel CCA. *Magn. Reson. Imaging*, 28(8):1095–103, 2010. doi:10.1016/j.mri.2009.12.016.

[53] M. D. Fox and M. E. Raichle. Spontaneous fluctuations in brain activity observed with functional magnetic resonance imaging. *Nat. Rev. Neurosci.*, 8(9):700–11, 2007. doi:10.1038/nrn2201.

[54] N. Moradi, P. LeVan, B. Akin, B. G. Goodyear, and R. C. Sotero. Holo-Hilbert spectral-based noise removal method for EEG high-frequency bands. *J Neurosci Methods*, 368:109470, 2022. doi:

10.1016/j.jneumeth.2021.109470.

[55] L. M. Jonkman, J. L. Kenemans, C. Kemner, M. N. Verbaten, and H. van Engeland. Dipole source localization of event-related brain activity indicative of an early visual selective attention deficit in ADHD children. *Clin Neurophysiol*, 115(7):1537–49, 2004. doi:10.1016/j.clinph.2004.01.022.